Stage-dependent proteomic alterations in aqueous humor of diabetic retinopathy patients based on data-independent acquisition and parallel reaction monitoring

Yeanqi Jin[1,2†], Junbin Liu[1†], Xueli Zhang[1,3,4], Liang Zhang[1], Ying Cui[1], Xiaoyang Luo[1], Haoxian Zhu[1,2], Zhifan Chen[5], Mengya Liu[1], Xiyu Wu[1], Xinyu Chen[1], Shuoxin Liao[1], Guanrong Wu[1], Xiang Fang[3*] and Qianli Meng[1*]

Abstract

Background Diabetic retinopathy (DR), a microvascular complication of diabetes mellitus (DM), represents the predominant cause of preventable vision loss in working-age populations globally. While the pathophysiological mechanisms underlying DR progression remain incompletely understood, our study employs comprehensive proteomic profiling of aqueous humor (AH) to identify stage-specific biomarkers and therapeutic targets in type 2 diabetes mellitus (T2DM) patients across DR progression.

Methods Utilizing data-independent acquisition (DIA) mass spectrometry, we quantified AH proteomes in a discovery cohort comprising 24 subjects: 18 T2DM patients stratified by DR severity [6 non-DR, 6 non-proliferative DR (NPDR), 6 proliferative DR (PDR)] and 6 cataract controls without diabetes (non-DM). Validation cohort analysis (including 10 AH samples in each group) was performed using parallel reaction monitoring (PRM) strategy for verification of target proteins. Comprehensive bioinformatics analyses included gene set enrichment analysis (GSEA), weighted gene co-expression network analysis (WGCNA), Kyoto encyclopedia of genes and genomes (KEGG) enrichment analysis, protein-protein interaction (PPI) network construction, receiver operating characteristic (ROC) curve analysis, and ConnectivityMap (Cmap)-based drug prediction.

Results Proteomic profiling identified 739 quantifiable AH proteins (62% extracellular) with clear separation among the four clinical stages in the discovery cohort. GSEA uncovered altered expression of proteins mainly related to complement and coagulation cascades, folate metabolism, and the selenium micronutrient network in patients with DR. WGCNA-derived protein modules yielded 83 PRM-validated targets, including 5 hub proteins differentiating NPDR from non-DR and 33 hub proteins showed significant upregulation in PDR versus NPDR comparison. Clinical correlation analysis identified F2, FGG, FGB, RBP4, AMBP, VTN, C8A, CPB2, and C2 associated with clinical traits. C6,

---

†Yeanqi Jin and Junbin Liu contributed equally to this work.

*Correspondence:
Xiang Fang
fangxiang@gdph.org.cn
Qianli Meng
mengqly@163.com
Full list of author information is available at the end of the article

FAM3C, SPP1, and JCHAIN levels were altered post-anti-VEGF treatment. Pharmacological prediction identified potential therapeutic compounds, including perindopril, triciribine, and XAV-939 for NPDR, and topiramate, triciribine, and vecuronium for PDR.

Conclusion This study established a comprehensive AH proteomic signature of DR progression, offering insights into the pathogenesis of DR and highlighting potential biomarkers and novel therapeutic targets.

Keywords Diabetic retinopathy, Aqueous humor, Proteomics, Data-independent acquisition, Parallel reaction monitoring

Background

Diabetes mellitus (DM) is a prevalent and rapidly growing global health issue, leading to severe complications and substantial healthcare expenses [1]. The 10th edition of the International Diabetes Federation (IDF) Diabetes Atlas estimates that the global diabetes prevalence in 20–79-year-olds in 2021 is 10.5% (536.6 million people), and will rise to 12.2% (783.2 million) in 2045 [2]. Diabetic retinopathy (DR), the most common and specific complication of DM, is the leading cause of preventable blindness in working adults worldwide [3]. The Global Burden of Disease Study identified DR as the fifth leading cause of blindness and moderate to severe vision impairment in individuals over 50 years of age [4]. Based on clinical findings, DR is categorized into no apparent retinopathy (non-DR), non-proliferative DR (NPDR), and proliferative DR (PDR) [5]. PDR, representing advanced stage of DR, can lead to irreversible visual impairment and blindness without treatment.

Accumulating evidence confirms that the pathogenesis of DR is multifactorial, involving oxidative stress, endothelial dysfunction, and inflammatory responses [6–8]. However, the underlying mechanisms and effective interventions remain unclear. Proteomic analysis, focusing on proteins as key disease effectors and drug targets, is instrumental in understanding disease-related protein functions. Consequently, several studies have attempted to identify potential biomarkers in various ocular fluids like vitreous humor (VH) [9, 10], aqueous humor (AH) [11, 12], or tear film [13], to elucidate the pathogenesis and explore therapeutic targets for DR. However, the findings from these studies have been inconsistent and often difficult to compare, potentially due to using different sample types, instrumentation, and analytical methodologies.

VH is commonly considered the priority sample to explore proteomic changes in DR because it is more closely related to retina than AH and tear film. However, VH proteomic analysis in clinical practice presents several challenges, including difficulty in sample collection, potential interference of vitreous hemorrhage, and limited availability of control samples. The AH plays a crucial role in various ocular pathophysiological processes. Despite the low concentration of proteins in AH compared to that of those in blood serum and VH, AH offers many advantages including a more accurate reflection of the ocular condition than blood serum, easier accessibility than VH, and greater stability than the tear film. A previous study reported that most proteins found in the VH were also observed in the AH of patients with PDR [14]. The abnormally expressed protein profiles in the AH from patients with DR may result from the leakage of proteins from the damaged retina and retinal blood vessels to the aqueous solution. Additionally, retinal proteins can leak into the cilia-retina circulation through disturbed blood-retinal and blood-aqueous barriers [15]. Therefore, AH may be a more suitable intraocular fluid for proteomic analysis. Its proteome profile not only represents the pathophysiological environment of the retina but can also be used to explore biomarkers for eye diseases.

In this study, we conducted a quantitative analysis of the AH proteome in patients with type 2 diabetes mellitus (T2DM) progressing from non-DR to PDR using mass spectrometry in data-independent acquisition (DIA) mode. Additionally, we identified differentially expressed proteins (DEPs) in patients with different stages of DR using a parallel reaction monitoring (PRM) strategy in an independent cohort. Through comprehensive proteomic data analysis, we aimed to elucidate potential mechanisms, identify biomarkers, and explore targets for DR.

Methods

Participants

All participants underwent comprehensive ophthalmic examinations at the Guangdong Provincial People's Hospital. According to the diabetic retinopathy disease severity scale and international diabetic retinopathy severity scale, patients with T2DM were classified into non-DR, NPDR, or PDR [5]. The inclusion criteria were as follows: (1) senile cataract patients without DM scheduled for phacoemulsification and intraocular lens implantation; (2) senile cataract patients with T2DM scheduled for phacoemulsification and intraocular lens implantation; (3) T2DM patients with DR scheduled for anti-vascular endothelial growth factor (VEGF) intravitreal injection. Exclusion criteria included the coexistence of other main ocular diseases, history of ophthalmic intervention

Jin *et al. Journal of Translational Medicine*   (2025) 23:476

Page 3 of 18

procedures (e.g., laser photocoagulation, anti-VEGF intravitreal injection, vitrectomy, cataract extraction), autoimmune diseases, malignant tumors, severe liver disease, or pregnancy. In the discovery cohort, 18 patients with T2DM including 6 without DR (non-DR group), 6 with NPDR (NPDR group), and 6 with PDR (PDR group); and 6 senile cataract patients without T2DM (non-DM group) were recruited for DIA analysis. In the validation cohort, 10 patients were enrolled in each of the four groups, and the key proteins selected from the DIA analysis were validated using the PRM approach. In addition, 10 AH samples from the PDR group after intravitreal anti-VEGF treatment (Conbercept, Kanghong Biotechnologies, Chengdu, China; PV group) were also collected during the pars plana vitrectomy surgery. Each AH sample (100–200 μL) was harvested from the anterior chamber during microscope-assisted surgery using a sterile 1 mL insulin injection syringe and needle, and immediately kept in storage at – 80 °C for subsequent analysis.

The clinical data, including age, gender, diabetes duration, body mass index (BMI), blood pressure, laboratory tests for hemoglobin A1c (HbA1c), serum total cholesterol (TC), triglycerides (TG), high-density lipoprotein cholesterol (HDL-C), low-density lipoprotein cholesterol (LDL-C), lipoprotein a, apolipoprotein (APO) A1, APOB100, serum creatinine, estimated glomerular filtrate rate (eGFR), international normalized ratio (INR), prothrombin activity (PT-A), prothrombin time (PT), activated partial thromboplastin time (APTT), fibrinogen (FIB), and thrombin time (TT) within one week of ophthalmic examinations were recorded. Demographic and clinical characteristics of the enrolled patients are summarized in Tables S1 and S2. Data are expressed as mean ± standard deviation (SD). Fisher's exact test and the Kruskal–Wallis H test were used to compare differences in clinical data using the R package TableOne (version 0.13.2) [16]. A *p*-value of < 0.05 was considered significant.

Data-dependent acquisition (DDA) library generation and mass spectrometry (MS) assay for DDA and DIA

AH samples were treated on ice using a high-intensity ultrasonic processor (Qsonica, Newtown, USA). Then samples from the discovery cohort were quantitatively examined using an MS assay for DIA. The most abundant proteins in the AH pools were separated on a Human 14 Multiple Affinity Removal System Column (Agilent Technologies, California, USA). High- and low-abundance proteins were collected, desalted, and concentrated using a 5 kDa ultrafiltration tube (Sartorius, Gottingen, Germany). SDT buffer (4% SDS, 100 mM Tris-HCl, pH 7.6) was added, boiled for 15 min, and centrifuged at 14,000 *g* at 4 °C for 20 min. The supernatant was quantified using the BCA Protein Assay Kit according to the

manufacturer's instructions (Bio-Rad, Hercules, California, USA).

Proteins were digested using a filter-aided sample preparation technique. Briefly, 200 μg protein extracts were put into an ultrafiltration tube. Low-molecular-weight components were removed using UA buffer (8 M urea in 100 mM Tris-HCl, pH 8.5) via repeated ultrafiltration. Then 100 μL of 11 mM iodoacetamide (I6125, Sigma-Aldrich, Saint Louis, USA) was added to block reduced cysteine residues and the samples were incubated for 30 min in darkness. The filters were washed thrice with UA buffer and then with 50 mM NH_4HCO_3 buffer (A6141, Sigma-Aldrich, Saint Louis, USA) twice. Finally, the protein suspensions were digested with trypsin (V5111, Promega, Madison, USA) at 1:50 trypsin-to-protein mass ratio overnight at 37 °C and 1:100 trypsin-to-protein mass ratio for a second 4 h digestion. The resulting peptides were collected as a filtrate, desalted on C18 cartridges (Thermo Fisher Scientific, Waltham, USA), concentrated using vacuum centrifugation, and reconstituted in 40 μL 0.1% formic acid (F0507, Sigma-Aldrich, Saint Louis, USA).

For DDA-MS analysis, all fraction samples were analyzed by TlMSTOF mass spectrometer (Bruker, Massachusetts, USA) connected to Evosep One system liquid chromatography (Evosep, Odense, Denmark). The MS was operated in a DDA mode for the ion mobility-enhanced spectral library generation. We set the accumulation and ramp time 100 ms each and recorded mass spectra in the range from *m/z* 100–1700 in positive electrospray mode, dynamic exclusion of 24.0s. Ion source Voltage was set at 1500 V, temperature at 180℃, and dry gas at 3 L/min. The ion mobility was scanned from 0.75 to 1.35 Vs/cm^2, then 8 cycles were performed with a 1.17 s duty cycle time using Parallel Accumulation-SErial Fragmentation (PASEF) MS/MS.

For DIA-MS analysis, the digested individual AH protein samples were analyzed by the same mass spectrometer and liquid chromatography as used in the DDA-MS analysis in the DIA mode. The mass spectrometer collected ion mobility MS spectra over a mass range of *m/z* 100–1700. We defined up to 4 windows for single 100 ms TlMS scans according to the m/z-ion mobility plane. During PASEF MS/MS scanning, the collision energy was ramped linearly as a function of the mobility from 20 eV at 1/K0 = 0.85 Vs/cm^2 to 59 eV at 1/K0 = 1.30 Vs/cm^2.

MS data analysis

For DDA library data, the FASTA sequence database was searched using the Spectronaut™ (version 14.4.200727.47784, http://www.biognosys.com/) against the Uniprot human database (Homo_sapiens_9606_SP_20 230 103," containing 20389 protein sequences), with trypsin specificity allowing one missed cleavage.

Carbamidomethylation (C) was set as a fixed modification, while oxidation (M) and acetylation (protein N-term) were set as dynamic modifications. A decoy database was introduced to calculate the FDR resulting from random matches. All reported data were based on 99% confidence for protein identification as determined by false discovery rate (FDR) < 1%.

The DIA data in the spectral library were analyzed using the Spectronaut™ (version 14.4.200727.47784). The main software parameters were as follows: retention time prediction type, dynamic iRT; interference with MS2 level correction, enabled; and cross-run normalization, enabled. The proteins in each sample were identified using peptide spectrum matching. All peptide and protein results were filtered based on a Q-value cutoff of 0.01 (equivalent to FDR < 1%).

Protein identification based on DIA mode

Proteins with quantitative data from more than 50% of the samples in each group were selected for further analysis. The cellular localization of each protein was evaluated using the DeepTMHMM server (https://services.healthtech.dtu.dk/services/DeepTMHMM-1.0/), a tool that predicts the transmembrane helices and the cellular localization of proteins based on their amino acid sequences. The predictions were further validated to ensure consistency with known protein localization data. To identify proteins associated with extracellular vesicles (EVs), the identified proteins were cross-referenced with the Vesiclepedia database, which is a comprehensive resource of proteins associated with EVs. The comparison was performed using the FunRich tool (https://funrich.org/) [17], which integrates various functional enrichment analyses. A Venn plot was used to show the overlapping proteins among the four groups. Three-dimensional principal component analysis (PCA) was performed and plotted using the R packages ropls (version 1.14.1) and scatterplot3d (version 0.3–41). Proteins with a fold change above 1.5 and a *p*-value less than 0.05 (Student's t-test) were considered differential proteins between the two groups. Statistical analyses were performed using SPSS (version 24.0; SPSS Inc., Chicago, IL, USA).

Gene set enrichment analysis (GSEA)

GSEA was performed using the GSEA software v3.1.0 (www.broadinstitute.org/gsea/index.jsp) against the canonical pathways downloaded from the MSigDB database (https://www.gsea-msigdb.org/gsea/msigdb/human/genesets.jsp?collection=CP) [18]. Gene sets with *p*-value less than 0.05 were considered significantly enriched. The visual representation of GSEA was generated using the R package GseaVis (version 0.1.0; https://github.com/junjunlab/GseaVis).

Weighted gene co-expression network analysis (WGCNA) and determination of the candidate proteins for PRM validation

The R package WGCNA (Version 1.68) was employed to cluster proteins with similar expression profiles and explore their association with clinical traits. The co-expression network was constructed through the following steps: (1) A hierarchical clustering analysis based on protein expression data was performed to exclude outliers. (2) A β value was selected as the weighting coefficient to build the adjacency matrix and a subsequent scale-free network. Next, the samples were clustered using the hierarchical clustering method and co-expressed modules were constructed using a dynamic tree-cutting algorithm. Core modules were screened based on an absolute correlation coefficient greater than 0.5 and a *p*-value less than 0.01. Modules with stronger correlations to clinical traits were further prioritized for downstream analysis.

Candidate proteins for PRM validation were identified through a two-step process: (1) Pearson correlation coefficients between module eigengenes and clinical traits were measured and modules significantly related to clinical traits (*p* < 0.05) were subjected to Kyoto encyclopedia of genes and genomes (KEGG) pathway enrichment analysis using the R package ClusterProfiler (version 4.10.1); (2) Pearson correlation coefficients (gene significance, GS) between protein expression levels and clinical traits, and module membership (MM) between protein expression levels and module eigengenes were calculated [19]. Candidate proteins in the modules positively correlated with clinical traits were filtered using GS values > 0.5 and MM values > 0.7, while those in negatively correlated modules were filtered with GS values < − 0.5 and MM values > 0.7.

PRM validation

AH samples from the validation cohort were quantitatively examined by LC-PRMMS analysis [20] to verify the expression levels of candidate proteins obtained by the DIA approach. Peptides were prepared following the DIA protocol and tryptic peptides were loaded onto C18 stage tips (5 μm particles, 4.6 mm ID, and 250 mm length) for desalting before reversed-phase chromatography on an Easy nLC-1200 system (Thermo Scientific, Massachusetts, USA). One hour liquid chromatography gradients with acetonitrile concentrations ranging from 5 to 30% in 45 min were used. PRM analysis was performed on a Q Exactive HF-X mass spectrometer (Thermo Scientific) with the following parameters: a full MS1 scan acquired with a resolution of 60,000 (at 300 m/z), AGC target 3.0×10^{-6}, and maximum ion injection time 200 ms. This was followed by 20 PRM scans at 30,000 resolution (at 200 m/z), AGC 3.0×10^{-6}, and a maximum injection time of 100 ms. Data were searched against Uniprot human
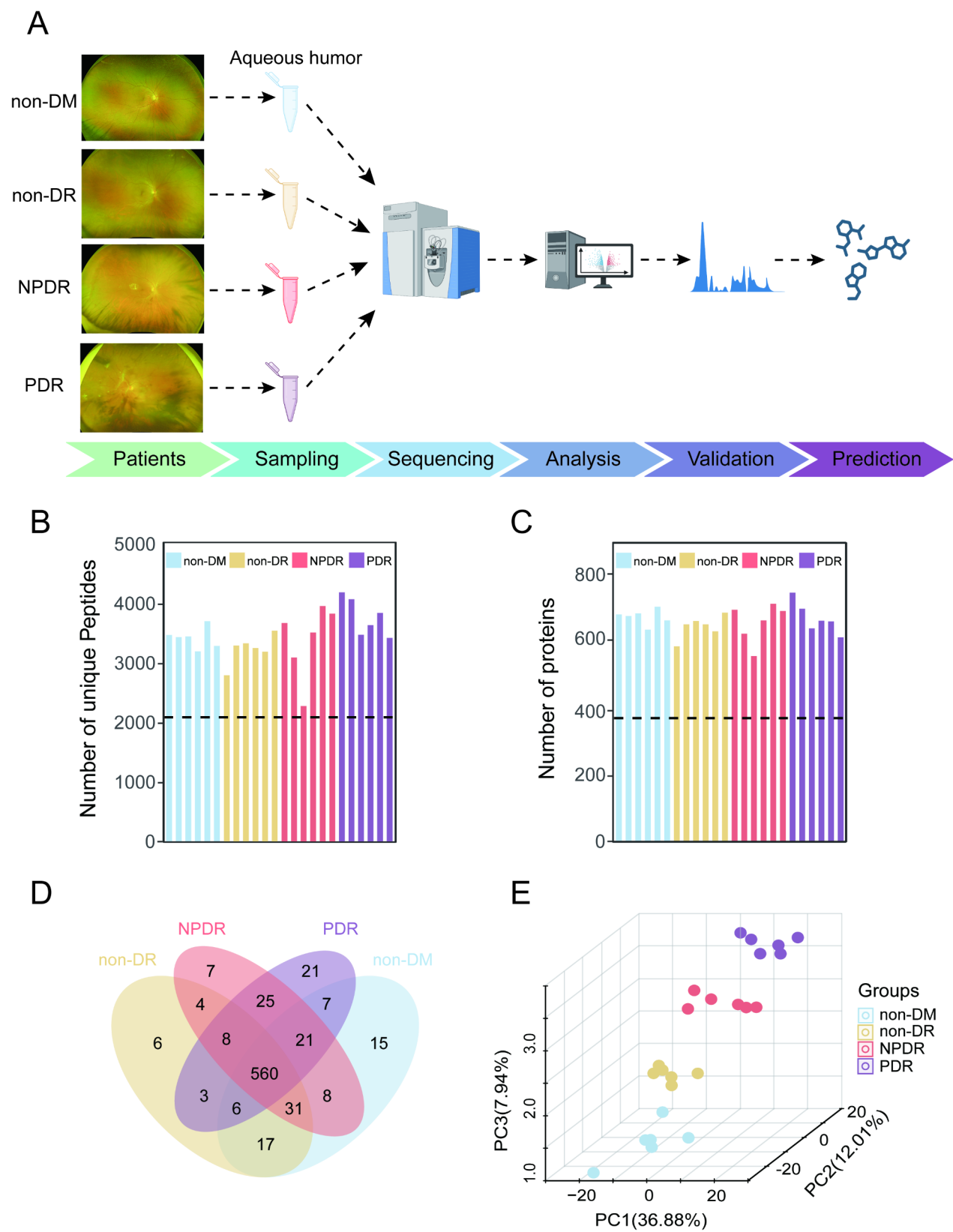
Fig. 1 (See legend on next page.)

(See figure on previous page.)

Fig. 1 Workflow of the study and protein identification in aqueous humor using DIA mode. (**A**) Overview of the study workflow. (**B**) Number of unique peptides examined in each sample. (**C**) Number of proteins identified in each sample. (**D**) Venn diagram showing unique proteins in aqueous humor from non-DM, non-DR, NPDR, and PDR groups. (**E**) PCA plots of non-DM, non-DR, NPDR, and PDR groups based on DIA analysis in the discovery cohort. DIA: data-independent acquisition; DM: diabetes mellitus; DR: diabetic retinopathy; NPDR: non-proliferative diabetic retinopathy; PDR: proliferative diabetic retinopathy; PCA: principal component analysis

database (Homo_sapiens_9606_SP_20 230 103.fasta) and analyzed using the Skyline protocol (MacCoss Lab, University of Washington) [21].

Proteins with a fold change above 1.5 and a *p*-value less than 0.05 in PRM were identified as differentially expressed proteins (DEPs). WikiPathways enrichment analysis for DEPs was performed using the R package ClusterProfiler (version 4.10.1). Pathways with a *p*-value < 0.05 were considered significantly enriched. A protein-protein interaction (PPI) network was constructed to examine the interrelations of the identified DEPs. The network was built using STRING DB (version 11) and visualized with Cytoscape (version 3.6.1). The interaction degree of each DEP was calculated to assess its significance within the network. Receiver operating characteristic (ROC) curve analysis was employed to evaluate the potential of DEPs to differentiate between various stages of DR using R Software 4.1.3. The area under curve (AUC) with a 95% confidence interval (CI) was calculated, and DEPs with AUC values of 0.7 or higher were considered hub proteins. Pearson correlation analysis was performed to assess the relationship between hub proteins and clinical data (including age, DM duration, BMI, and laboratory test indicators). In addition, a paired sample t-test was conducted using SPSS version 24.0 (SPSS, Inc., Chicago, IL, USA) to compare changes in DEPs between PDR and PV groups following anti-VEGF treatment.

ConnectivityMap (CMap)-based drug prediction

The CMap database (https://clue.io/) was employed to identify compounds that produce signatures opposite to those induced by NPDR vs. non-DM and PDR vs. non-DM [22]. Upregulated proteins between NPDR and non-DM, as well as between PDR and non-DM were used for analysis. The parameters used included gene expression (L1000), the touchstone reference dataset, individual query, and version 1.0. A list of compounds was generated, ordered by their similarity to the input signature, with scores ranging from −100 to 100. A negative score indicated an opposing effect between the compound and the input signature. The top fifteen compounds with a score < −99 and known mechanism of action were retained for further analysis.

Results

AH spectral library generation and protein identification by DIA

In this study, the library was constructed by DDA-MS analysis, including all spectrums of non-DM, non-DR, NPDR, and PDR groups (Fig. 1A). A total of 5800 peptides and 795 proteins were obtained by DIA-MS analysis. From these, 739 proteins having quantitative data in over 50% of samples from each group were used for further analysis (Fig. 1B-C, Table S3). Of these 739 proteins, 456 (62%) were extracellular, 156 (21%) intracellular, and 127 (17%) transmembrane proteins (Fig. S1). Additionally, among the 283 intracellular and transmembrane proteins, 237 (84%) were classified as vesicle proteins (Table S3). The non-DM, non-DR, NPDR, and PDR groups contained 665, 635, 664, and 651 proteins, respectively, with 560 proteins common to all groups (Fig. 1D). Three-dimensional PCA analysis of AH protein expression profiles demonstrated clear separation among the four clinical stages, indicating overall heterogeneity (Fig. 1E).

Differential proteomic analysis among the four groups identified 244 differential proteins (82 upregulated, 162 downregulated) in DR vs. non-DR, 104 (42 upregulated, 62 downregulated) in NPDR vs. non-DR, 124 (35 upregulated, 89 downregulated) in PDR vs. NPDR, and 23 (7 upregulated, 16 downregulated) in non-DR vs. non-DM (Fig. S2).

Protein enrichment analysis

Next, we performed GSEA to investigate the molecular mechanisms at various stages of DR. Compared to the non-DR group, the upregulated differential proteins in the DR group exhibited significant enrichment in folate metabolism, selenium micronutrient network, complement and coagulation cascades, and transport of small molecules pathways, while the downregulated differential proteins were enriched in the metabolism of carbohydrates and lysosome pathways. Similar protein-enriched pathways were noted in the PDR vs. NPDR comparison. However, in the NPDR vs. non-DR comparison, upregulated pathways included binding and uptake of ligands by scavenger receptors instead of the transport of small molecules, while downregulated pathways involved Rho Gtpase effectors and membrane trafficking. Moreover, compared to the non-DR group, the differential proteins of AH, were enriched in signaling by Wnt, Rho Gtpase

effectors and cell cycle pathways, which showed a markedly decreasing trend in the non-DM group (Fig. 2).

Protein co-expression modules

WGCNA analysis was conducted to identify the core modules and key proteins whose expression was closely associated with the clinical traits. Five protein co-expression modules were identified: turquoise (237 proteins), blue (202 proteins), brown (65 proteins), grey (74 proteins), and yellow (43 proteins). The turquoise, brown, and blue modules were core modules (Table S4, Fig. S3). The turquoise module correlated positively with PDR (cor = 0.72, p = 8e-05), with proteins enriched in complement and coagulation cascades, glycolysis/gluconeogenesis, and cholesterol metabolism (Fig. 3A-D). The blue (cor = − 0.78, p = 8e-06) with proteins enriched in the lysosome and cell adhesion molecule and brown modules (cor = − 0.66, p = 4e-04) with proteins enriched in

estrogen signaling pathways and pathways of neurodegeneration-multiple diseases correlated negatively with PDR. Candidate proteins identified based on GS and MM values were 76, 100, and 31 for the turquoise, blue, and brown modules, respectively (Fig. 3E-G).

Analysis of DEP characteristics by PRM validation

Based on their potential biological relevance to DR and combined with fold change analysis, 96 proteins were further selected from the candidate proteins identified by WGCNA for PRM validation in an independent cohort. PRM analysis confirmed 83 proteins (51 in turquoise, 30 in blue, and 2 in brown) in the validation cohort (Table S5). Seven DEPs were detected in the NPDR vs. non-DR groups, with five (F2, KLKB1, FGG, APCS, and FGB) having AUC values above 0.7 (Table 1, Table S6, Fig. 4A, Fig. S4A). KEGG analysis indicated these DEPs were enriched in complement and coagulation cascades, folate
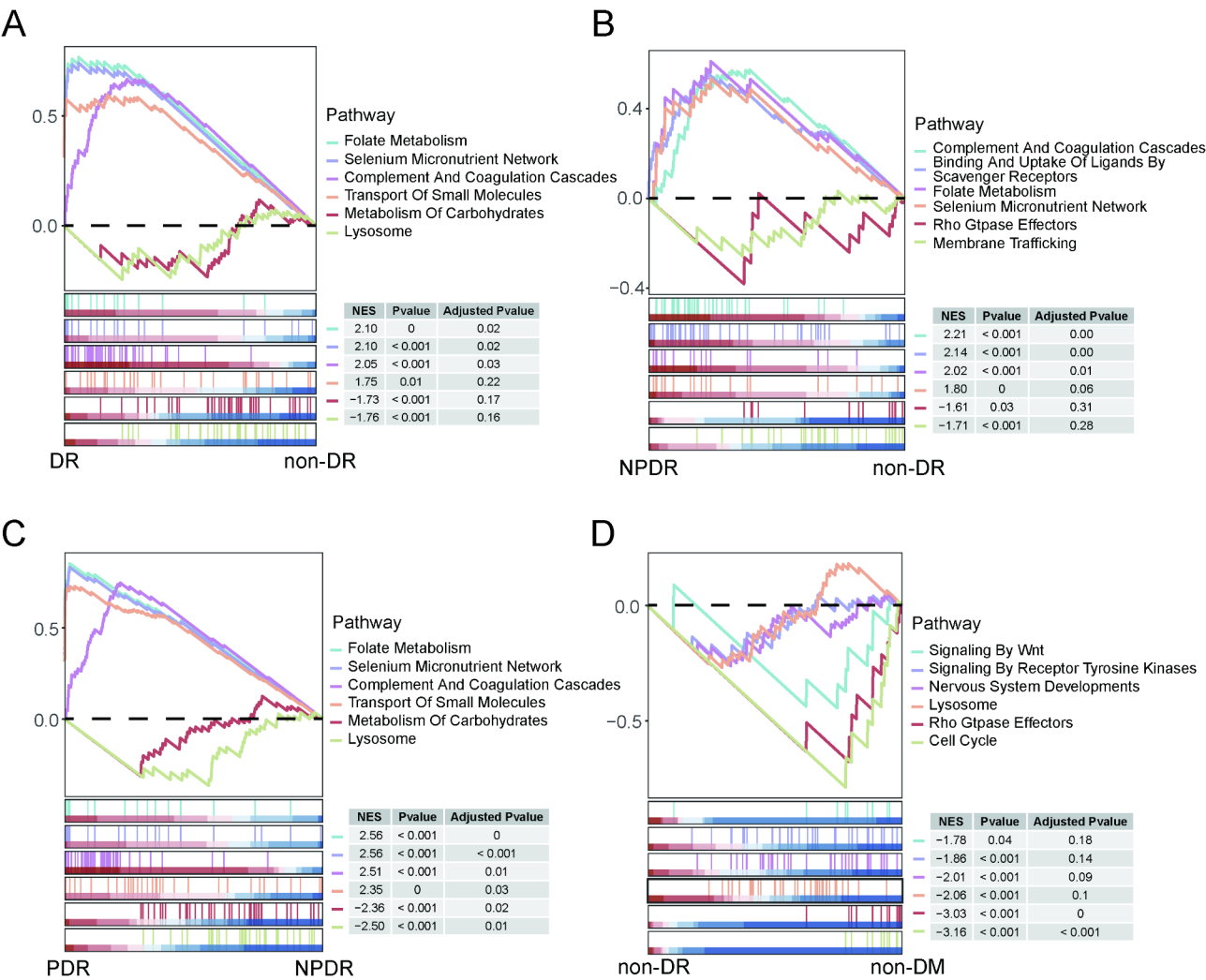

Fig. 2 Key enriched pathways in DR vs. non-DR (**A**), NPDR vs. non-DR (**B**), PDR vs. NPDR (**C**) and non-DR vs. non-DM (**D**) using GSEA. DM: diabetes mellitus; DR: diabetic retinopathy; NPDR: non-proliferative diabetic retinopathy; PDR: proliferative diabetic retinopathy; GSEA: gene set enrichment analysis
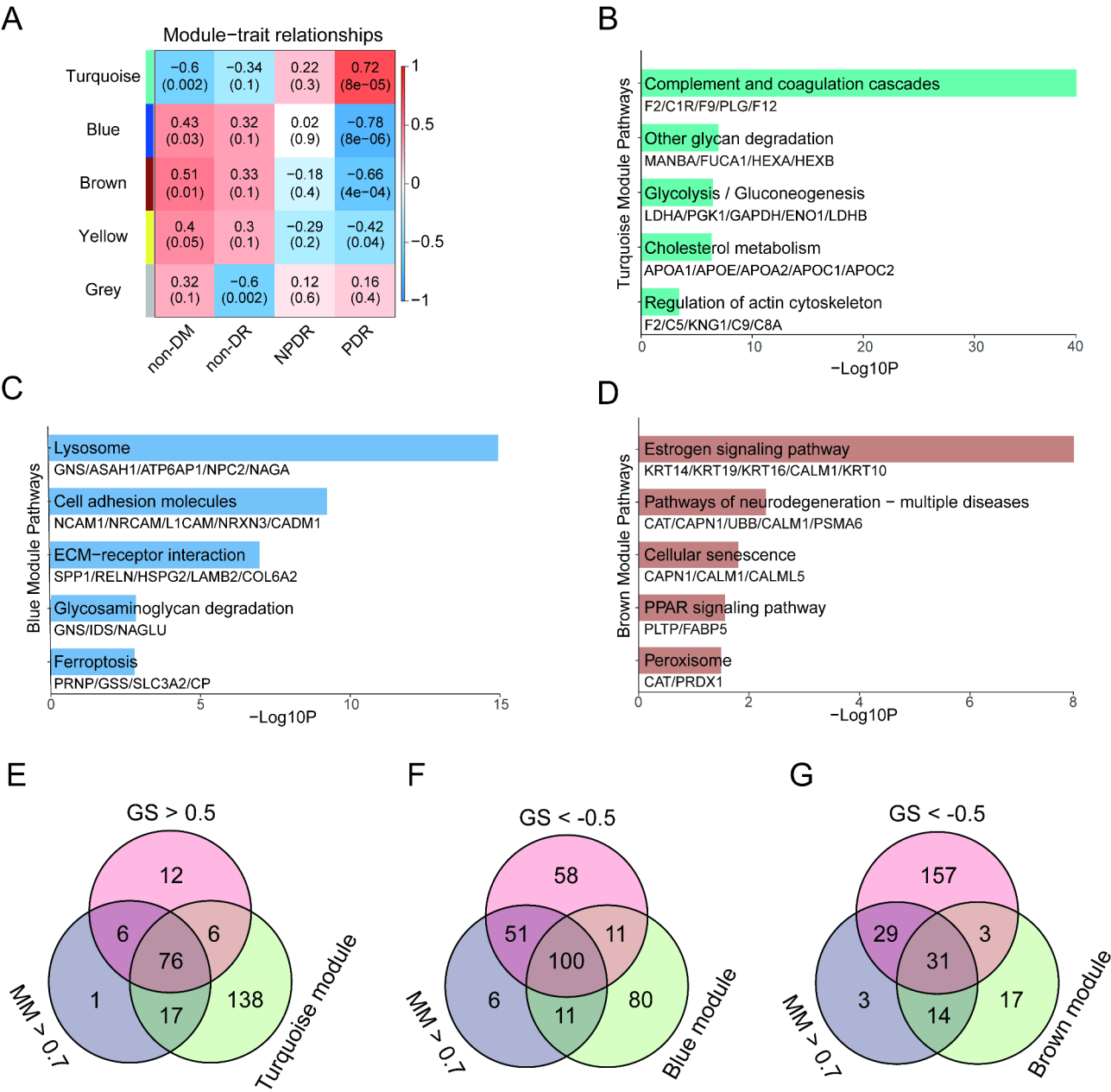
Fig. 3 Identification of clinically significant protein modules by weighted correlation network analysis. (**A**) Module-trait correlation plot based on module eigengenes, where red and blue represent positive and negative correlations, respectively. Values in each grid represent the correlation coefficient and corresponding *p*-value in parentheses between modules and clinical traits. (**B**–**D**) KEGG analysis of the turquoise (**B**), blue (**C**), and brown (**D**) modules. (**E**) Venn diagram showing proteins with GS (PDR) > 0.5 and MM > 0.7 in the turquoise module. (**F**, **G**) Venn diagram showing proteins with GS (PDR) < −0.5 and MM > 0.7 in the (**F**) blue and (**G**) brown modules. WGCNA: weighted correlation network analysis; KEGG: Kyoto Encyclopedia of Genes and Genomes; GS: gene significance; MM: module membership

metabolism, selenium micronutrient network, VEGFA VEGFR2 signaling, and vitamin B12 metabolism. PPI analysis revealed interactions among the five hub proteins (Fig. 4B,C, Table S7).

Thirty-three DEPs (all with AUC > 0.7) were significantly upregulated in the PDR vs. NPDR groups were corroborated in the validation cohort using PRM (Table S6). The top 10 hub proteins were C8A, RBP4, CPB2,

VTN, AMBP, C2, PLG, AFM, C6, and F2 (Table 1; Fig. 4D, Fig. S4B). These DEPs were mainly enriched in complement and coagulation cascades, allograft rejection, cells and molecules involved in local acute inflammatory response, angiotensin II receptor type 1 pathway, and vitamin B12 metabolism. PPI ranked by degree identified F2, C3, PLG, AMBP, and VTN as the core proteins (Fig. 4E,F, Table S7).

Table 1 The hub proteins (ranked by AUC) in NPDR vs. non-DR and PDR vs. NPDR

Protein	Gene name	Protein location	module	Ratio	*P* value	AUC value
NPDR vs. non-DR						
P00734	F2	extracellular	turquoise	1.54009	0.036444	0.89
P03952	KLKB1	extracellular	turquoise	2.155632	0.010474	0.86
P02679	FGG	extracellular	turquoise	12.65522	0.033686	0.79
P02743	APCS	extracellular	turquoise	3.336828	0.035931	0.78
P02675	FGB	extracellular	turquoise	8.553475	0.044983	0.77
PDR vs. NPDR						
P07357	C8A	extracellular	turquoise	2.222135	0.000302	0.94
P02753	RBP4	extracellular	turquoise	4.09654	0.000158	0.93
Q96IY4	CPB2	extracellular	turquoise	2.497397	0.001473	0.92
P04004	VTN	extracellular	turquoise	2.516913	0.007644	0.92
P02760	AMBP	extracellular	turquoise	3.088958	0.002747	0.91
P06681	C2	extracellular	turquoise	2.054174	0.006503	0.91
P00747	PLG	extracellular	turquoise	2.060559	0.000463	0.90
P43652	AFM	extracellular	turquoise	2.737774	0.004905	0.89
P13671	C6	extracellular	turquoise	2.938061	0.000725	0.89
P00734	F2	extracellular	turquoise	1.806203	0.002592	0.89

AUC, area under curve; non-DR, without diabetic retinopathy; NPDR, non-proliferative diabetic retinopathy; PDR, proliferative diabetic retinopathy.

Correlation analysis between deps and clinical traits

Next, we analyzed the relationship between the hub proteins and clinical data. Among the five hub proteins of the NPDR vs. non-DR groups, F2 and FGG were significantly correlated with HbA1c (F2: $R = 0.68$, $p = 0.030$; FGG: $R = 0.74$, $p = 0.014$), INR (F2: $R = 0.72$, $p = 0.019$; FGG: $R = 0.69$, $p = 0.027$), PT (F2: $R = 0.77$, $p = 0.009$; FGG: $R = 0.74$, $p = 0.015$), and TT (F2: $R = 0.71$, $p = 0.023$; FGG: $R = 0.73$, $p = 0.017$). In addition, F2 also had a negative correlation with PT-A ($R = -0.67$, $p = 0.036$), and FGB was positively associated with PT ($R = 0.68$, $p = 0.031$) (Fig. 5A). No association was found between APCS and KLKBI and the clinical data.

In the PDR vs. NPDR groups, 6 of the top 10 hub proteins (RBP4, AMBP, VTN, C8A, CPB2, and C2) were associated with clinical traits (Fig. 5B). RBP4 showed a positive correlation with lipoprotein a ($R = 0.68$, $p = 0.030$). AMBP was negatively correlated with eGFR ($R = -0.69$, $p = 0.041$), and positively correlated with FIB ($R = 0.65$, $p = 0.040$). VTN also showed a positive correlation with FIB ($R = 0.64$, $p = 0.044$). C8A, CPB2, and C2 were closely related to coagulation indices APTT, INR, PT, and PT-A.

Protein characteristics before and after anti-VEGF treatment

To explore the response of proteins identified in the validation cohort by PRM to anti-VEGF treatment, we compared changes in patients with PDR before and after anti-VEGF treatment. Among the 83 DEPs validated by PRM, C6 and FAM3C were significantly decreased, whereas SPP1 and JCHAIN were substantially increased post-treatment. The remaining 79 DEPs, including 31 hub proteins from the PDR vs. NPDR groups, showed no significant changes (Fig. 6).

Drug prediction for NPDR and PDR

To investigate potential new drugs for NPDR and PDR treatment, bioactive compounds mimicking the effects observed in NPDR vs. non-DM groups and PDR vs. non-DM groups were retrieved from the CMap database. Two lists of 2429 compounds, scored from −100 to 100, were obtained. The top 15 compounds (score < −99) for NPDR and PDR were identified, based on the principle that negative values indicate the reversion of the signature expression (Tables S8-S9). A systematic literature review of PubMed database revealed the strong therapeutic efficacy of triciribine (an AKT inhibitor) and perindopril (an ACE inhibitor) for NPDR in animal studies. Additionally, we identified BRD-K41143549, XAV-939, and AS-604850, which have mechanisms of action similar to a glutamate receptor antagonist, a tankyrase inhibitor, and a PI3K inhibitor, respectively, might have potential therapeutic benefit for NPDR (Fig. 7B and C). For PDR, triciribine and topiramate (a carbonic anhydrase inhibitor) demonstrated promising results by literature, while vecuronium (an acetylcholine receptor antagonist), O-1918 (a cannabinoid receptor antagonist), RO-60-0175 (a serotonin receptor agonist), CAY-10577 and CAY-10578 (both casein kinase inhibitors), and LY-341495 (a glutamate receptor antagonist) might also be potential therapeutic candidates base on our findings (Fig. 7B and D).
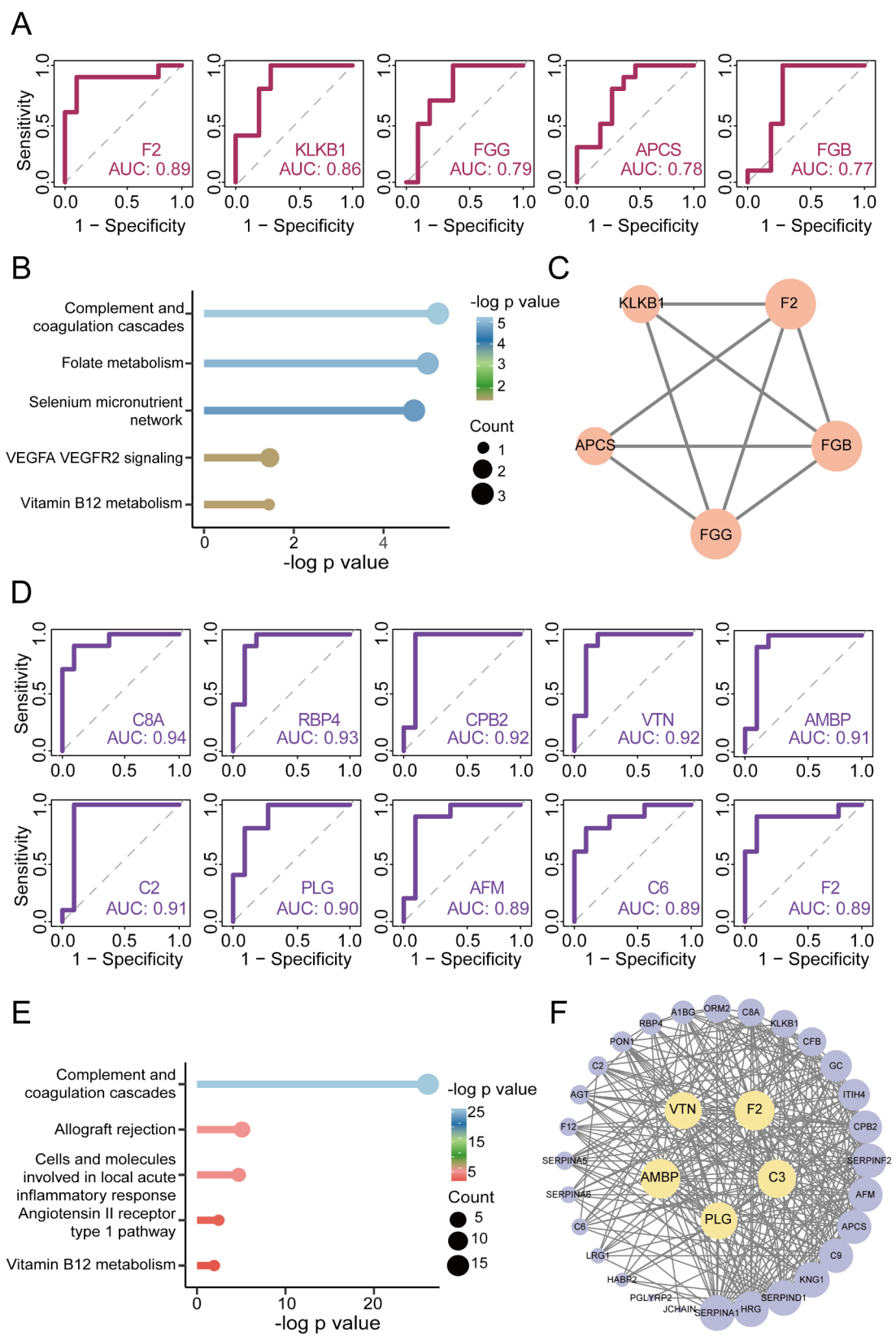
Fig. 4 (See legend on next page.)

(See figure on previous page.)

Fig. 4 PRM-based validation in an independent cohort. (**A**) ROC curves show the ability of the top five hub proteins (ranked by AUC) to distinguish NPDR from non-DR. (**B**) Lollipop diagram showing key pathways enriched for the seven DEPs from NPDR vs. non-DR. (**C**) PPI network of the five hub proteins from NPDR vs. non-DR. (**D**) ROC curves show the ability of the top ten hub proteins (ranked by AUC) to distinguish PDR from NPDR. (**E**) Lollipop diagram showing key pathways enriched for the 33 DEPs from PDR *vs*. NPDR. (**F**) PPI network of the 33 DEPs from PDR *vs*. NPDR. PRM: parallel reaction monitoring; ROC: receiver operating characteristic; AUC: area under curve; DEPs: differentially expressed proteins; PPI: protein-protein interaction; DR: diabetic retinopathy; NPDR: non proliferative diabetic retinopathy; PDR: proliferative diabetic retinopathy

Discussion

The present study delineates the quantitative proteomic profile of the AH at different stages of DR using DIA-based analysis and PRM-based validation. The DIA analysis identified 739 comparable AH proteins and critical molecular pathways involved in DR progression, including the complement and coagulation cascades, folate metabolism, and selenium micronutrient network. The hub proteins implicated in the occurrence and development of DR were screened using PRM validation, and F2, FGG, FGB, RBP4, AMBP, VTN, C8A, CPB2, and C2 of them were associated with clinical traits. Additionally, C6, FAM3C, SPP1, and JCHAIN levels were altered post-anti-VEGF treatment. Finally, potential therapeutic drugs for NPDR and PDR, including triciribine, perindopril and topiramate, were predicted.

Our findings exhibit partial concordance with previous studies. For instance, a mass spectrometry-based label-free quantitative proteomics study identified 10 DEPs in VH from PDR vs. NPDR groups, including APOB, APOC3, HABP2, CD14, ITIH4, CPN2, APOM, AMBP, C1QB, and FAM3C [10], which were also detected in our AH analysis. A recent proteomic study of AH liquid biopsies reported an overlap of 60 out of 1784 DEPs in DR vs. controls with our findings [12]. Additionally, APOC4, AMBP and IGHA1 were identified in both tear and AH from Chinese patients with DR [13].

GSEA revealed upregulated pathways related to folate metabolism and the selenium micronutrient network in the AH patients with DR, compared to that in those without DR. This finding suggests increased metabolic activity of folate and selenium, leading to higher consumption of these elements in the eyes of the patients with DR. Both folic acid and selenium can suppress inflammation and oxidative stress, with supplementation shown to partially prevent DR [23–26]. Consistent with previous studies on intraocular fluid of DR [9–12], our findings also revealed upregulation of complement and coagulation cascades in patients with DR, suggesting these pathways may be activated through multiple mechanisms during DR development. Complement and coagulation are related to proteolytic cascades in the blood. Dysregulation of the complement system can cause tissue damage, pathological inflammation, and coagulation activation. Hyperactivation of the complement system is linked to diseases like glomerulonephritis and systemic lupus erythematosus [27, 28], while inactivation is associated with

conditions like septicemia and endotoxemia [29]. The abnormal coagulation cascade is involved in hematological [30], cardiovascular [31], liver [32], and nervous system diseases [33]. Accumulating evidence suggests that cross-talk exists between the complement system and the coagulation cascade. A recent study showed that platelets in the tumor microenvironment can promote tumor cell invasion and metastasis by activating the coagulation cascade, and inhibit immune cell cytotoxicity by activating the complement system [34]. In contrast, pathways related to the metabolism of carbohydrates and lysosomes were downregulated in the AH of patients with DR. This indicates that the intraocular glucose metabolic capacity was reduced, affecting the growth, metabolism, and survival of cells.

Increasing evidence indicates that WGCNA can not only explore network module structures, measure the relationships between genes and modules, explore the relationships among modules, and rank ordered genes or modules, but also generate testable hypotheses for validation in independent datasets [35, 36]. Therefore, we selected candidate proteins based on WGCNA for PRM validation in an independent cohort. The ROC curve analysis of NPDR vs. non-DR suggested that F2, KLKB1, FGG, APCS, and FGB may serve as biomarkers for distinguishing retinopathy in patients with diabetes. These proteins were enriched in complement and coagulation cascades, folate metabolism, and selenium micronutrient network pathways. Moreover, three of these proteins (F2, FGG, and FGB) correlated with coagulation indices like PR-INR, PT, TT, and PT-A. F2, also known as prothrombin, converts to thrombin during coagulation, serving as a key enzyme in the blood-clotting cascade [37]. It is upregulated in patients with diabetes and may contribute to atherothrombotic complications in T2DM [38]. FGG and FGB, the gamma and beta chains of fibrinogen respectively, play crucial roles in hemostasis, wound healing, and vascular pathology [39]. They are also differentially expressed in the umbilical vessels of patients with gestational diabetes mellitus, indicating that intrauterine hyperglycemia is associated with an elevated cardiovascular risk in the offspring [40]. Additionally, F2 and FGG were positively correlated with HbA1c, suggesting that the coagulation cascade is involved in diabetic control or progression. KLKB1 is activated to kallikrein, which in turn activates factor XII and participates in the intrinsic coagulation pathways. The kallikrein system has
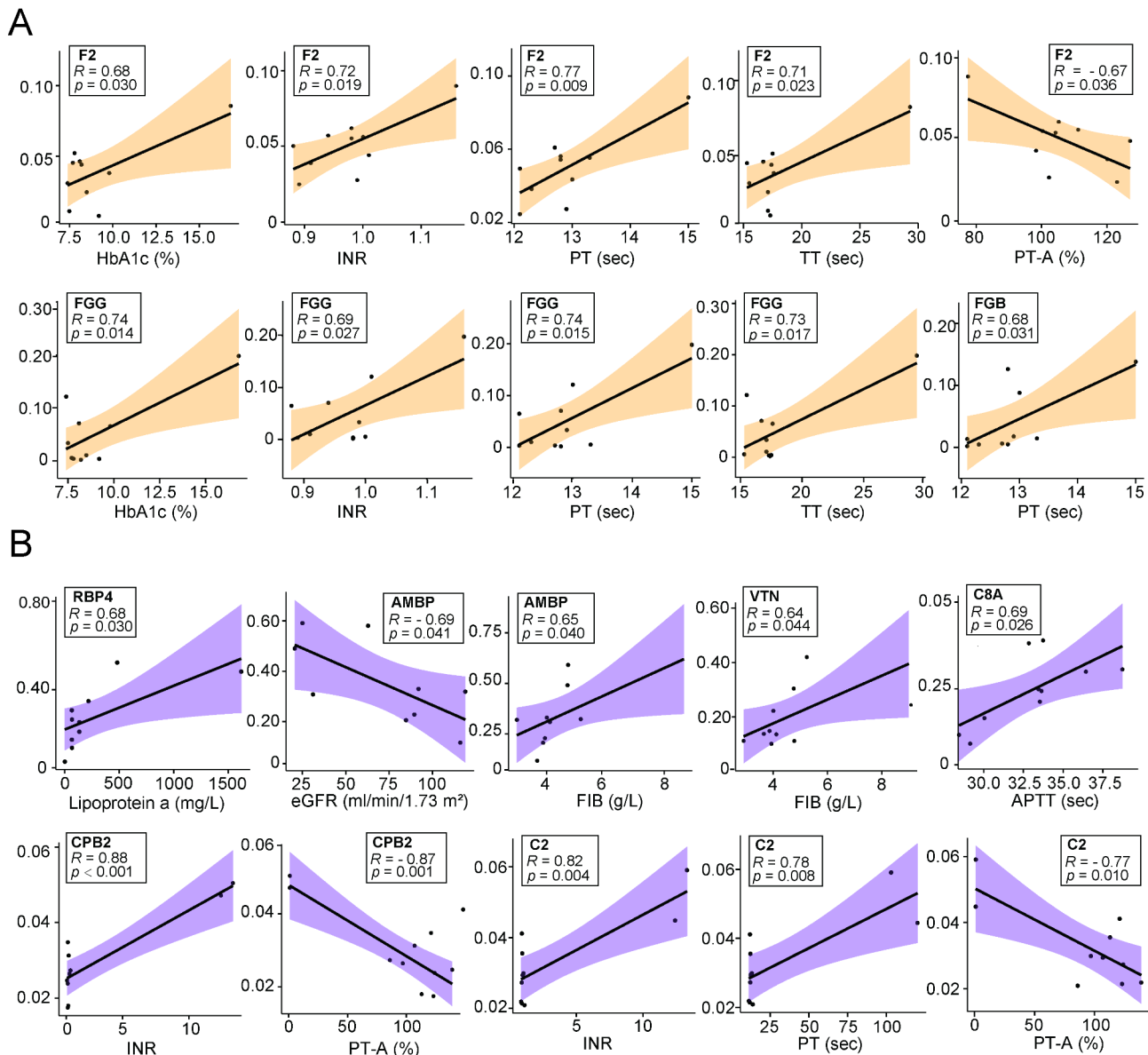
Fig. 5 Pearson correlation analysis between hub proteins and clinical traits. (**A**) F2, FGG, and FGB from NPDR vs. non-DR are significantly correlated with clinical data. (**B**) RBP4, AMBP, VTN, C8A, CPB2, and C2 from the top ten hub proteins in PDR vs. NPDR are significantly correlated with clinical data. DR: diabetic retinopathy; NPDR: non-proliferative diabetic retinopathy; PDR: proliferative diabetic retinopathy

been reported as a VEGF-independent mediator of diabetic macular edema (DME) [41]. APCS is a naturally occurring homopentameric plasma protein that is highly conserved across species and acts as a soluble pattern recognition receptor in the innate immune system, with functions including the regulation of matrix formation and complement activation [42]. Nevertheless, further studies are required to elucidate the relationship between these proteins and DR.

The 33 identified hub proteins, primarily enriched in complement and coagulation cascades, may differentiate between NPDR and PDR. Among the top ten proteins by AUC values (C8A, RBP4, CPB2, VTN, AMBP, C2, PLG, AFM, C6, and F2), five (VTN, AMBP, PLG, C2, and F2) were core proteins in the PPI network, and six (RBP4, AMBP, VTN, C8A, CPB2, and C2) were associated with lipoprotein, renal function, and coagulation indices. RBP4, positively associated with lipoprotein a, regulates lipid metabolism and insulin sensitivity, contributing to DR progression as a novel proangiogenic factor [43, 44]. Moreover, RBP4 stimulates proinflammatory cytokines like IL-6 and ICAM-1 in endothelial cells, promotes leukocyte adherence [45], increases mitochondrial superoxide production, and induces apoptosis [46]. AMBP cleaved into alpha-1-microglobulin and bikunin, both of which participate in various biological processes
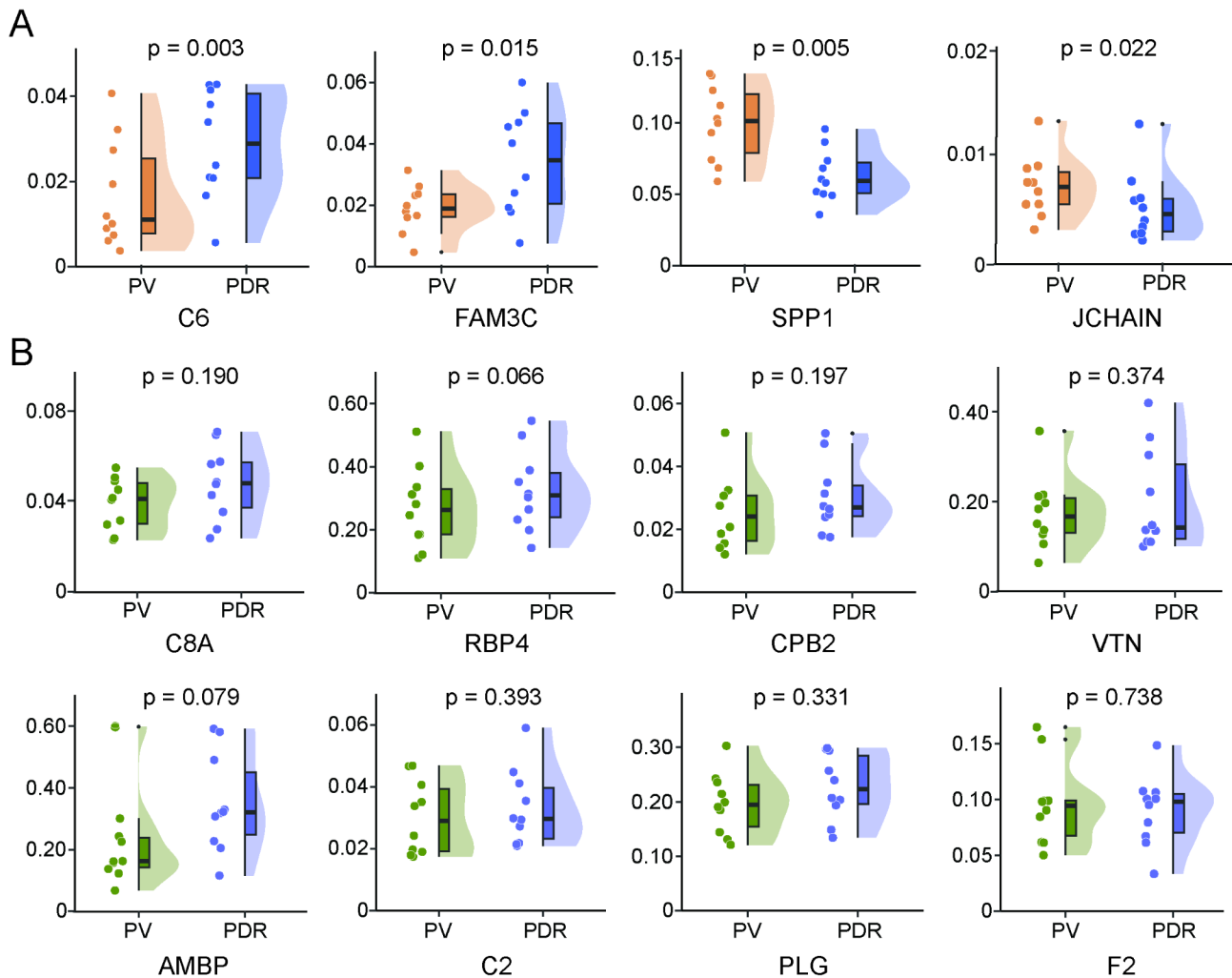
Fig. 6 Raincloud plots show the response of hub proteins validated by PRM in PDR patients after anti-VEGF treatment. (**A**) C6 and FAM3C are significantly decreased, while SPP1 and JCHAIN are significantly increased after anti-VEGF treatment. (**B**) Eight of the top ten hub proteins between PDR and NPDR show no changes after anti-VEGF treatment. PRM: parallel reaction monitoring; PDR: proliferative diabetic retinopathy; VEGF: vascular endothelial growth factor

such as cell growth, cellular calcium uptake, and inflammation [47]. It is considered a biomarker distinguishing healthy individuals from patients with nephropathy and those with and without diabetic nephropathy [48], which is similar to our result that AMBP exhibited a negative correlation with eGFR. Although AMBP showed a positive correlation with FIB, its role in the coagulation cascade remains unclear. In this study, VTN, C8A, CPB2, and C2 correlated with coagulation indices. VTN, an extracellular matrix protein, is involved in cell adhesion, blood coagulation, and fibrinolysis [49, 50]. It has been reported to distinguish glaucoma from cataract with significant upregulation in glaucoma [51, 52], and also acts as a hub protein in the AH proteomes of PDR [52]. C8A is a subunit of the C8 complex in the complement system, which is a component of the membrane attack complex (MAC) [53]. To our knowledge, there are no reports

on the association between C8A and DR or other diabetes-related complications. CPB2, or thrombin-activatable fibrinolysis inhibitor (TAFI), is crucial in coagulation and fibrinolysis [54], and has recently been identified as a potential protein marker closely linked to the progression of DR [55]. C2, a key component of the classical complement pathway, plays a crucial role in inflammatory responses [56] and shows significant alteration in the PDR group compared to dry age-related macular degeneration [57]. Our findings suggest that F2 is likely involved in DR progression as a hub protein both in the PDR vs. NPDR comparison and in the NPDR vs. non-DR comparison. Consequently, we speculate that intervention targeting these hub proteins may have potential therapeutic effects in NPDR or PDR.

Despite the widespread use of anti-VEGF-based therapy for DME and PDR, approximately 40% of patients
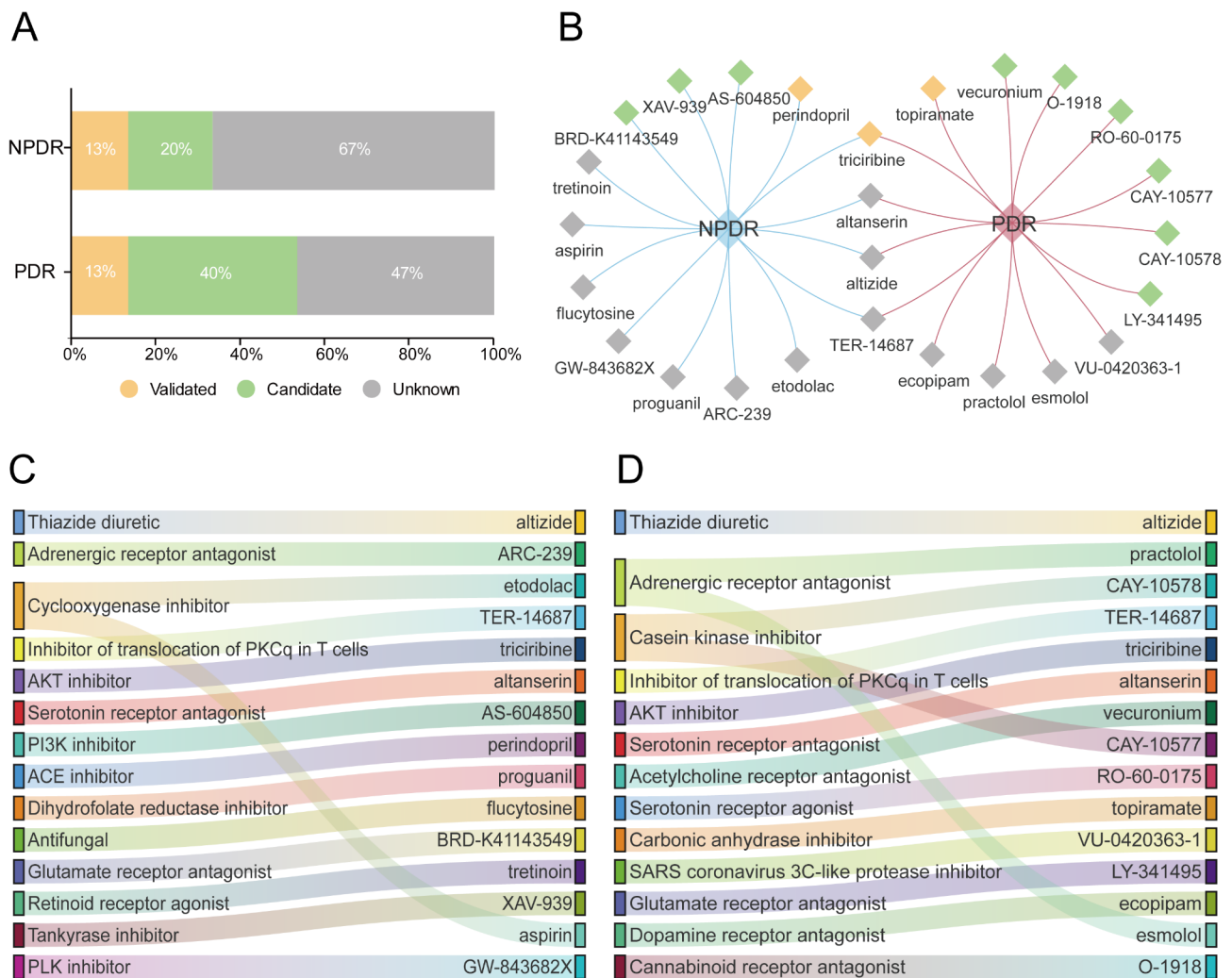
Fig. 7 CMap-based drug repurposing analysis for NPDR and PDR. (**A**) Barplot indicating the percentage of 15 predicted compounds for NPDR and PDR. Drugs validated in animal experiments, agents sharing common mechanisms of action with known drugs, and compounds with undetermined functions for DR are represented by orange, blue, and gray, respectively. (**B**) Venn diagram illustrating the shared and unique compounds for NPDR and PDR. (**C**, **D**) Mechanisms of action (MOA) of predicted drugs are represented in Sankey diagrams for NPDR (**C**) and PDR (**D**). NPDR: non-proliferative diabetic retinopathy; PDR: proliferative diabetic retinopathy

with DME show a poor response, indicating the potential involvement of molecules other than VEGF [58, 59]. Our study revealed a significant decrease in C6 and FAM3C and an increase in SPP1 and JCHAIN levels post-anti-VEGF treatment. C6 is part of the complement system and participates in MAC formation [60]. Anti-C6 antibodies have been shown to suppress MAC formation and significantly lower both the incidence and progression of choroidal neovascularization (CNV) in a mouse model [61]. SPP1, or OPN, is a secreted phosphoprotein involved in cell adhesion, signal transduction, and immune regulation [62]. SPP1 interacts with cancer-associated genes such as *VEGF*, *FGA*, *JUN*, *EGFR*, and *TGFB1* [63]. A recent in vivo study demonstrated that $Spp1^+$ macrophages express a proangiogenic transcriptome through VEGF signaling, endothelial cell sprouting,

cytokine signaling, and fibrosis [64]. Our findings indicated that C6 levels, positively correlated with PDR, significantly decreased after anti-VEGF treatment, while SPP1 levels, negatively correlated with PDR, significantly increased, suggesting that anti-VEGF treatment may affect these proteins, apart from disrupting VEGF–VEGF receptor interactions.

FAM3C, also known as interleukin-like epithelial-mesenchymal transition (EMT) inducer, plays a role in EMT, which significantly affects cancer cell invasion and migration [65, 66]. JCHAIN links monomeric IgA and IgM into dimers or polymers, facilitating their transport across epithelial cells and thus contributing to mucosal immunity [67]. Our findings showed that FAM3C was negatively correlated with PDR and significantly decreased after anti-VEGF treatment, whereas JCHAIN

was positively correlated with PDR and significantly increased after anti-VEGF therapy. These findings suggest that anti-VEGF therapy may simultaneously activate other signaling pathways. Except for C6 and JCHAIN, the other 31 hub proteins in PDR vs. NPDR comparison showed no significant change. This duality may explain the poor response in some patients after anti-VEGF treatment and suggests these proteins as potential intervention targets for PDR.

The CMap query tool has been used to effectively screen candidate drugs in proteomics data [68, 69]. Herein we utilized it to predict potential inhibitors for NPDR and PDR using our AH proteome data. Perindopril, an ACE inhibitor used in hypertension management [70], has been shown to mitigate DR in diabetic rats [71], aligning with our predictions. Similarly, a glutamate receptor antagonist, known for its use in Alzheimer's disease [72], has demonstrated protective effects in DR mice by reducing ROS/TXNIP/NLRP3 signaling [73], suggesting BRD-K41143549 as a potential therapeutic agent against DR. Although Tankyrase inhibitor is primarily investigated for Wnt-pathway dependent cancers [74], a recent study indicated that it could regulate naïve diabetic human iPSCs to generate vascular progenitors for efficient revascularization of ischemic retina [75], suggesting that Tankyrase inhibitor XAV-939 might protect against DR. Hyperactivation of the PI3K signaling pathway, associated with tumorigenesis and resistance to treatment in various cancer types, and the inhibitors of this pathway thus are as potential antitumor drugs [76]. Additionally, the PI3K inhibitor AS-604850 ameliorated joint inflammation and damage in mouse models of arthritis and lupus; [77, 78] and was also predicted to be effective against NPDR in our study, likely due to the involvement of inflammatory response in DR.

Triciribine, an AKT inhibitor, has demonstrated synergistic efficacy with multiple therapeutic against various malignancies [79]. Our findings regarding the potency of Triciribine in preventing NPDR and PDR corroborate a previous study showing its ability to mitigate pathological neovascularization and reduce vascular permeability in a mouse model of proliferative retinopathy [80]. Topiramate, a carbonic anhydrase inhibitor approved for epilepsy treatment and migraine prophylaxis [81], was predicted in our study markedly attenuated PDR, consistent with previous experimental evidence demonstrating its neuroprotective effects against excitotoxicity and ischemic injury in rat retinas [82]. Studies have demonstrated the efficiency of acetylcholine receptor antagonists against DME [83] and cannabinoid receptor blockade against vascular inflammation and cell death in DR [84]. Moreover, serotonin receptor agonists protect the retina from severe photo-oxidative damage [85], whereas casein kinase 2 inhibitors remarkably suppress preretinal

neovascularization in a proliferative retinopathy mouse model [86]. Therefore, the therapeutic potential of the predicted drugs, including Vecuronium (a neuromuscular blocking agent) [87], O-1918, RO-60-0175 (an agent for reducing addiction to cocaine) [88], along with CAY-10577 and CAY-10578, warrants further investigation for PDR treatment.

To thoroughly explore the proteomic characteristics of AH in DR, our study employed two key measures: precise sample grouping based on the clinical features of DR, and detection of the AH proteome using the DIA mode, followed by key protein validation via the PRM approach. Furthermore, the alterations in protein expression before and after anti-VEGF therapy were assessed, as well as the potential therapeutic drugs were predicted, which providing a valuable basis for the management of DR. However, this study has several limitations. Firstly, the number of clinical samples analyzed was limited. Considering that the consistency of the samples is easily influenced by individual differences, further studies with larger cohorts are necessary to better identify biomarkers and differentiate DR stages. Secondly, DIA- or PRM-based proteomic technologies have certain limitations. For instance, VEGF-A and IL-6, known to be involved in PDR, were not detected in our study, likely due to their small molecular weight and low abundance. Moreover, current proteomic techniques remain imperfect. More than 200 whole proteins obtained by DIA and 13 of the 83 key proteins validated by PRM in our study were not detected in a recently reported study by Wolf et al., [12] that identified 5,953 proteins in AH using an aptamer-based proteomics assay. Thirdly, the biological functions of the hub proteins require further exploration using cell and animal models. Lastly, the drug predictions for NPDR and PDR were descriptive and their efficacy needs to be validated in some models.

Conclusions

In conclusion, our study comprehensively analyzed the proteomic characteristics of AH across different stages of DR, focusing on signaling pathways, hub proteins, and potential therapeutic agents. We identified additional hub proteins in the AH that distinguish PDR from NPDR, indicating that abnormal changes and interactions of various functional proteins in the eye are crucial to DR progression. This underscores the importance of exploring ocular biomarkers and the potential for discovering novel drug targets. Our findings offer insights into the mechanisms of DR, identify biomarkers for clinical diagnosis, and guide the development of more effective treatments.

Abbreviations
AH   Aqueous humor
APO   Apolipoprotein
APTT   Activated partial thromboplastin time

AUC	Area under curve
BMI	Body mass index
CI	Confidence interval
Cmap	ConnectivityMap
DDA	Data-dependent acquisition
DEPs	Differentially expressed proteins
DIA	Data-independent acquisition
DM	Diabetes mellitus
DME	Diabetic macular edema
DR	Diabetic retinopathy
eGFR	Estimated glomerular filtrate rate
FIB	Fibrinogen
GS	Gene significance
GSEA	Gene set enrichment analysis
HbA1c	Hemoglobin A1c
HDL-C	High-density lipoprotein cholesterol
IDF	International Diabetes Federation
INR	International normalized ratio
KEGG	Kyoto encyclopedia of genes and genomes
LDL-C	Low-density lipoprotein cholesterol
MM	Module membership
MS	Mass spectrometry
NPDR	Non-proliferative diabetic retinopathy
PCA	Principal component analysis
PDR	Proliferative diabetic retinopathy
PPI	Protein-protein interaction
PRM	Parallel reaction monitoring
PT	Prothrombin time
PT-A	Prothrombin activity
ROC	Receiver operating characteristic
SD	Standard deviation
T2DM	Type 2 diabetes mellitus
TC	Total cholesterol
TG	Triglycerides
TT	Thrombin time
VEGF	Vascular endothelial growth factor
VH	Vitreous humor
WGCNA	Weighted gene co-expression network analysis

Supplementary Information

The online version contains supplementary material available at https://doi.org/10.1186/s12967-025-06452-z.

Supplementary Material 1

Supplementary Material 2

Supplementary Material 3

Supplementary Material 4

Supplementary Material 5

Supplementary Material 6

Supplementary Material 7

Supplementary Material 8: Figure S1: Cellular localization of the 739 identified proteins in aqueous humor. (A) The proportions of extracellular, intracellular, and transmembrane proteins. (B) Major constituent proteins among transmembrane proteins.

Supplementary Material 9

Supplementary Material 10

Supplementary Material 11: Figure S2: Multi-group difference scatter plot showing counts of differential proteins in DR vs. non-DR, NPDR vs. non-DR, PDR vs. NPDR, non-DR vs. non-DM. DR: diabetic retinopathy; NPDR: non-proliferative diabetic retinopathy; PDR: proliferative diabetic retinopathy; DM: diabetes mellitus.

Supplementary Material 12: Figure S3: Scale-free topology checking and module construction in WGCNA. (A) Scale independence analysis across

a spectrum of soft threshold powers (1–20) to determine the optimal transformation. The red line represents the scale-free topology criterion. (B) Mean connectivity analysis across a spectrum of soft threshold powers, showing the decay of mean connectivity following an inverse power law. (C) Hierarchical clustering dendrogram illustrating five distinct modules of highly co-expressed proteins (turquoise, blue, brown, grey, and yellow). WGCNA: weighted correlation network analysis.

Supplementary Material 13: Figure S4 Comparative analysis of protein expression profiles by PRM quantification. (A) Statistical comparison of the 5 hub proteins (based on AUC values) between NPDR vs. non-DR groups. (B) Statistical comparison of the top 10 hub proteins (based on AUC values) between PDR and NPDR groups. PRM: parallel reaction monitoring; AUC: area under curve; DR: diabetic retinopathy; NPDR: non-proliferative diabetic retinopathy; PDR: proliferative diabetic retinopathy.

Data availability
The datasets generated and/or analysed during the current study have been deposited to the ProteomeXchange Consortium (http://proteomecentral.proteomexchange.org) via the iProX partner repository with the dataset identifier PXD046630 (for DIA) and PXD053634 (for PRM).

Declarations

Ethics approval and consent to participate
This study was conducted following the tenets of the Declaration of Helsinki and approved by the Research Ethics Committee of Guangdong Provincial People's Hospital (KY2024-516-02). All participants provided written informed consent.

Consent for publication
All authors give their consent for publication of this manuscript.

Competing interests
The authors declare that they have no competing interests.

Author details
[1]Department of Ophthalmology, Guangdong Eye Institute, Guangdong Provincial People's Hospital (Guangdong Academy of Medical Sciences), Southern Medical University, Guangzhou, China
[2]School of Medicine, South China University of Technology, Guangzhou, China
[3]Medical Research Institute, Guangdong Provincial People's Hospital (Guangdong Academy of Medical Sciences), Southern Medical University, Guangzhou, China
[4]Guangdong Provincial Key Laboratory of Artificial Intelligence in Medical Image Analysis and Application, Guangzhou, China
[5]The Fourth Affiliated Hospital of Guangzhou Medical University, Guangzhou, China

References

1. Heald AH, Stedman M, Davies M, Livingston M, Alshames R, Lunt M, et al. Estimating life years lost to diabetes: outcomes from analysis of National diabetes audit and office of National statistics data. Cardiovasc Endocrinol Metabolism. 2020;9(4):183–5.
2. Sun H, Saeedi P, Karuranga S, Pinkepank M, Ogurtsova K, Duncan BB, et al. IDF diabetes atlas: global, regional and country-level diabetes prevalence estimates for 2021 and projections for 2045. Diabetes Res Clin Pract. 2022;183:109–19.
3. Cheung N, Mitchell P, Wong TY. Diabetic retinopathy. Lancet (London England). 2010;376(9735):124–36.
4. Causes of blindness and vision impairment. In 2020 and trends over 30 years, and prevalence of avoidable blindness in relation to VISION 2020: the right to sight: an analysis for the global burden of disease study. Lancet Global Health. 2021;9(2):e144–60.
5. Flaxel CJ, Adelman RA, Bailey ST, Fawzi A, Lim JI, Vemulakonda GA, et al. Diabetic Retinopathy Preferred Practice Pattern® Ophthalmol. 2020;127(1):P66–145.
6. Kang Q, Yang C. Oxidative stress and diabetic retinopathy: molecular mechanisms, pathogenetic role and therapeutic implications. Redox Biol. 2020;37:101799.
7. Sorrentino FS, Matteini S, Bonifazzi C, Sebastiani A, Parmeggiani F. Diabetic retinopathy and endothelin system: microangiopathy versus endothelial dysfunction. Eye (Lond). 2018;32(7):115
8. Semeraro F, Cancarini A, dell'Omo R, Rezzola S, Romano MR, Costagliola C. Diabetic retinopathy: vascular and inflammatory disease. J Diabetes Res. 2015;2015:582060.
9. Wang J, Wang Z, Zhang Y, Li J. Proteomic analysis of vitreal exosomes in patients with proliferative diabetic retinopathy. Eye (Lond). 2023;37:2061–8.
10. Loukovaara S, Nurkkala H, Tamene F, Gucciardo E, Liu X, Repo P, et al. Quantitative proteomics analysis of vitreous humor from diabetic retinopathy patients. J Proteome Res. 2015;14(12):5131–43.
11. Wang T, Chen H, Du X, Li N, Chen Y, Min H. Differences in aqueous humor protein profiles in patients with proliferative diabetic retinopathy before and after conbercept treatment. J Proteom. 2023;276:104838.
12. Wolf J, Rasmussen DK, Sun YJ, Vu JT, Wang E, Espinosa C, et al. Liquid-biopsy proteomics combined with AI identifies cellular drivers of eye aging and disease in vivo. Cell. 2023;186(22):4868–e48844812.
13. Fan Z, Hu Y, Chen L, Lu X, Zheng L, Ma D, et al. Multiplatform tear proteomic profiling reveals novel non-invasive biomarkers for diabetic retinopathy. Eye (Lond). 2024;38(8):1509–17.
14. Balaiya S, Zhou Z, Chalam KV. Characterization of vitreous and aqueous proteome in humans with proliferative diabetic retinopathy and its clinical correlation. Proteom Insights. 2017;8:1178641816686078.
15. Freddo TF. A contemporary concept of the blood-aqueous barrier. Prog Retin Eye Res. 2013;32:181–95.
16. Panos A, Mavridis D. TableOne: an online web application and R package for summarising and visualising data. Evid Based Ment Health. 2020;23(3):127–30.
17. Fonseka P, Pathan M, Chitti SV, Kang T, Mathivanan S. FunRich enables enrichment analysis of omics datasets. J Mol Biol. 2021;433(11):166747.
18. Subramanian A, Tamayo P, Mootha VK, Mukherjee S, Ebert BL, Gillette MA, et al. Gene set enrichment analysis: a knowledge-based approach for interpreting genome-wide expression profiles. Proc Natl Acad Sci U S A. 2005;102(43):15545–50.
19. Yu G, Wang L-G, Han Y, He Q-Y. ClusterProfiler: an R package for comparing biological themes among gene clusters. OMICS. 2012;16(5):284–7.
20. Peterson AC, Russell JD, Bailey DJ, Westphall MS, Coon JJ. Parallel reaction monitoring for high resolution and high mass accuracy quantitative, targeted proteomics. Mol Cell Proteom. 2012;11(11):1475–88.
21. MacLean B, Tomazela DM, Shulman N, Chambers M, Finney GL, Frewen B, et al. Skyline: an open source document editor for creating and analyzing targeted proteomics experiments. Bioinf (Oxford England). 2010;26(7):966–8.
22. Subramanian A, Narayan R, Corsello SM, Peck DD, Natoli TE, Lu X, et al. A next generation connectivity map: L1000 platform and the first 1,000,000 profiles. Cell. 2017;171(6):1437–e14521417.
23. Gu J, Lei C, Zhang M. Folate and retinal vascular diseases. BMC Ophthalmol. 2023;23(1):413.
24. Lei XW, Li Q, Zhang JZ, Zhang YM, Liu Y, Yang KH. The protective roles of folic acid in preventing diabetic retinopathy are potentially associated with suppressions on angiogenesis, inflammation, and oxidative stress. Ophthalmic Res. 2019;62(2):80–92.
25. Bardak H, Uğuz AC, Bardak Y, Rocha-Pimienta J, Delgado-Adámez J, Espino J. Selenium protects ARPE-19 and ACBRI 181 cells against high Glucose-Induced oxidative stress. Molecules. 2023;28(16).
26. Niu T, Shi X, Liu X, Wang H, Liu K, Xu Y. Porous Se@SiO(2) nanospheres alleviate diabetic retinopathy by inhibiting excess lipid peroxidation and inflammation. Molecular medicine (Cambridge, Mass). 2024;30(1):24.
27. Kaartinen K, Safa A, Kotha S, Ratti G, Meri S. Complement dysregulation in glomerulonephritis. Semin Immunol. 2019;45:101331.
28. Lazar S, Kahlenberg JM. Systemic lupus erythematosus: new diagnostic and therapeutic approaches. Annu Rev Med. 2023;74:339–52.
29. Garred P, Tenner AJ, Mollnes TE. Therapeutic targeting of the complement system: from rare diseases to pandemics. Pharmacol Rev. 2021;73(2):792–827.
30. Cappellini MD. Coagulation in the pathophysiology of hemolytic anemias. Hematol Am Soc Hematol Educ Program. 2007:74–8.
31. Ząbczyk M, Ariëns RAS, Undas A. Fibrin clot properties in cardiovascular disease: from basic mechanisms to clinical practice. Cardiovasc Res. 2023;119(1):94–111
32. Argemi J, Kedia K, Gritsenko MA, Clemente-Sanchez A, Asghar A, Herranz JM, et al. Integrated transcriptomic and proteomic analysis identifies plasma biomarkers of hepatocellular failure in Alcohol-Associated hepatitis. Am J Pathol. 2022;192(12):1658–69.
33. Ma S-X, Seo BA, Kim D, Xiong Y, Kwon S-H, Brahmachari S, et al. Complement and coagulation cascades are potentially involved in dopaminergic neuro-degeneration in α-Synuclein-Based mouse models of Parkinson's disease. J Proteome Res. 2021;20(7):342
34. Oncul S, Cho MS. Interactions between platelets and tumor microenvironment components in ovarian cancer and their implications for treatment and clinical outcomes. Cancers 2023;15(4).
35. Langfelder P, Horvath S. WGCNA: an R package for weighted correlation network analysis. BMC Bioinformatics. 2008;9:559.
36. Zhang F-L, Li W-D, Zhang G, Zhang M, Liu Z-J, Zhu K-X, et al. Identification of unique transcriptomic signatures through integrated multispecies comparative analysis and WGCNA in bovine oocyte development. BMC Genomics. 2023;24(1):265.
37. Abrams ST, Su D, Sahraoui Y, Lin Z, Cheng Z, Nesbitt K, et al. Assembly of alternative prothrombinase by extracellular histones initiates and disseminates intravascular coagulation. Blood. 2021;137(1):103–14.
38. De Cristofaro R, Rocca B, Vitacolonna E, Falco A, Marchesani P, Ciabattoni G, et al. Lipid and protein oxidation contribute to a prothrombotic state in Patients with type 2 diabetes mellitus. J Thromb Haemost. 2003;1(2):250–6.
39. Laurens N, Koolwijk P, de Maat MPM. Fibrin structure and wound healing. J Thromb Haemost. 2006;4(5):932–9.
40. Pan HT, Xiong YM, Zhu HD, Shi XL, Yu B, Ding HG, et al. Proteomics and bioinformatics analysis of cardiovascular related proteins in offspring exposed to gestational diabetes mellitus. Front Cardiovasc Med. 2022;9:1021112.
41. Kita T, Clermont AC, Murugesan N, Zhou Q, Fujisawa K, Ishibashi T, et al. Plasma Kallikrein-Kinin system as a VEGF-Independent mediator of diabetic macular edema. Diabetes. 2015;64(10):3588–99.
42. Cox N, Pilling D, Gomer RH. Serum amyloid P: a systemic regulator of the innate immune response. J Leukoc Biol. 2014;96(5):739–43.
43. Li JY, Chen XX, Lu XH, Zhang CB, Shi QP, Feng L. Elevated RBP4 plasma levels were associated with diabetic retinopathy in type 2 diabetes. Biosci Rep. 2018;38(5).
44. Han W, Wei H, Kong W, Wang J, Yang L, Wu H. Association between retinol binding protein 4 and diabetic retinopathy among type 2 diabetic patients: a meta-analysis. Acta Diabetol. 2020;57(10):1203–18.
45. Farjo KM, Farjo RA, Halsey S, Moiseyev G, Ma JX. Retinol-binding protein 4 induces inflammation in human endothelial cells by an NADPH oxidase- and nuclear factor kappa B-dependent and retinol-independent mechanism. Mol Cell Biol. 2012;32(24):5103–15.
46. Wang J, Chen H, Liu Y, Zhou W, Sun R, Xia M. Retinol binding protein 4 induces mitochondrial dysfunction and vascular oxidative damage. Atherosclerosis. 2015;240(2):335–44.
47. Huang H, Han Y, Gao J, Feng J, Zhu L, Qu L et al. High level of serum AMBP is associated with poor response to paclitaxel-capecitabine chemotherapy in advanced gastric cancer patients. Medical oncology (Northwood, London, England). 2013;30(4):748.
48. Liao WL, Chang CT, Chen CC, Lee WJ, Lin SY, Liao HY et al. Urinary proteomics for the early diagnosis of diabetic nephropathy in Taiwanese patients. J Clin Med. 2018;7(12).
49. Preissner KT, Reuning U. Vitronectin in vascular context: facets of a multitalented matricellular protein. Semin Thromb Hemost. 2011;37(4):408–24.

50. Zuchtriegel G, Uhl B, Pick R, Ramsauer M, Dominik J, Mittmann LA, et al. Vitronectin stabilizes intravascular adhesion of neutrophils by coordinating B2 integrin clustering. Haematologica. 2021;106(10):2641–53.

51. Liu X, Liu X, Wang Y, Sun H, Guo Z, Tang X, et al. Proteome characterization of glaucoma aqueous humor. Mol Cell Proteomics: MCP. 2021;20:100117.

52. Wang T, Chen H, Li N, Zhang B, Min H. Aqueous humor proteomics analyzed by bioinformatics and machine learning in PDR cases versus controls. Clin Proteomics. 2024;21(1):36.

53. Couves EC, Gardner S, Voisin TB, Bickel JK, Stansfeld PJ, Tate EW, et al. Structural basis for membrane attack complex Inhibition by CD59. Nat Commun. 2023;14(1):890.

54. Leung LLK, Morser J. Carboxypeptidase B2 and carboxypeptidase N in the crosstalk between coagulation, thrombosis, inflammation, and innate immunity. Journal of thrombosis and haemostasis: JTH. 2018.

55. Wang S, Xia K, Zhu X, Liu Y, Sun L, Zhu Q. Separation of high-purity plasma extracellular vesicles for investigating proteomic signatures in diabetic retinopathy. J Chromatogr A. 2024;1718:464700.

56. Lintner KE, Wu YL, Yang Y, Spencer CH, Hauptmann G, Hebert LA, et al. Early components of the complement classical activation pathway in human systemic autoimmune diseases. Front Immunol. 2016;7:36.

57. Santos FM, Ciordia S, Mesquita J, Cruz C, Sousa J, Passarinha LA, et al. Proteomics profiling of vitreous humor reveals complement and coagulation components, adhesion factors, and neurodegeneration markers as discriminatory biomarkers of vitreoretinal eye diseases. Front Immunol. 2023;14:1107295.

58. Bressler SB, Ayala AR, Bressler NM, Melia M, Qin H, Ferris FL 3, et al. Persistent macular thickening after Ranibizumab treatment for diabetic macular edema with vision impairment. JAMA Ophthalmol. 2016;134(3):278–85.

59. Gonzalez VH, Campbell J, Holekamp NM, Kiss S, Loewenstein A, Augustin AJ, et al. Early and Long-Term responses to Anti-Vascular endothelial growth factor therapy in diabetic macular edema: analysis of protocol I data. Am J Ophthalmol. 2016;172:72–9.

60. Liu X, Wang Y, Bauer AT, Kirschfink M, Ding P, Gebhardt C, et al. Neutrophils activated by membrane attack complexes increase the permeability of melanoma blood vessels. Proc Natl Acad Sci USA. 2022;119(33):e2122716119.

61. Bora PS, Sohn JH, Cruz JM, Jha P, Nishihori H, Wang Y, et al. Role of complement and complement membrane attack complex in laser-induced choroidal neovascularization. J Immunol (Baltimore Md: 1950). 2005;174(1):491–7.

62. Rosmus DD, Lange C, Ludwig F, Ajami B, Wieghofer P. The role of osteopontin in microglia biology: current concepts and future perspectives. Biomedicines 2022;10(4).

63. Annadurai Y, Easwaran M, Sundar S, Thangamani L, Meyyazhagan A, Malaisamy A, et al. SPP1, a potential therapeutic target and biomarker for lung cancer: functional insights through computational studies. J Biomol Struct Dyn. 2024;42(3):1336–51.

64. Droho S, Rajesh A, Cuda CM, Perlman H, Lavine JA. CD11c+macrophages are proangiogenic and necessary for experimental choroidal neovascularization. JCI Insight. 2023;8(7).

65. Kim S, Oh J, Park C, Kim M, Jo W, Kim CS, et al. FAM3C in cancer-Associated adipocytes promotes breast cancer cell survival and metastasis. Cancer Res. 2024;84(4):545–59.

66. Thuya WL, Kong LR, Syn NL, Ding LW, Cheow ESH, Wong RTX, et al. FAM3C in Circulating tumor-derived extracellular vesicles promotes non-small cell lung cancer growth in secondary sites. Theranostics. 2023;13(2):621–38.

67. Kawasaki K, Ohta Y, Castro CD, Flajnik MF. The Immunoglobulin J chain is an evolutionarily co-opted chemokine. Proc Natl Acad Sci USA. 2024;121(3):e2318995121.

68. Wu L, Zhou L, An J, Shao X, Zhang H, Wang C, et al. Comprehensive profiling of extracellular vesicles in uveitis and scleritis enables biomarker discovery and mechanism exploration. J Transl Med. 2023;21(1):388.

69. Masson SWC, Madsen S, Cooke KC, Potter M, Vegas AD, Carroll L, et al. Leveraging genetic diversity to identify small molecules that reverse mouse skeletal muscle insulin resistance. Elife. 2023;12:RP86961.

70. Syed YY. Perindopril/Indapamide/Amlodipine in hypertension: A profile of its use. Am J Cardiovasc Drugs. 2022;22(2):219–30

71. Zheng Z, Chen H, Ke G, Fan Y, Zou H, Sun X, et al. Protective effect of Perindopril on diabetic retinopathy is associated with decreased vascular endothelial growth factor-to-pigment epithelium-derived factor ratio: involvement of a mitochondria-reactive oxygen species pathway. Diabetes. 2009;58(4):954–64.

72. Revett TJ, Baker GB, Jhamandas J, Kar S. Glutamate system, amyloid ß peptides and Tau protein: functional inter relationships and relevance to alzheimer disease pathology. J Psychiatry Neurosci. 2013;38(1):6–23.

73. ElSayed MH, Elbayoumi KS, Eladl MA, Mohamed AAK, Hegazy A, El-Sherbeeny NA, et al. Memantine mitigates ROS/TXNIP/NLRP3 signaling and protects against mouse diabetic retinopathy: histopathologic, ultrastructural and Bioinformatic studies. Biomed Pharmacother. 2023;163:114772.

74. Huang S-MA, Mishina YM, Liu S, Cheung A, Stegmeier F, Michaud GA, et al. Tankyrase Inhibition stabilizes Axin and antagonizes Wnt signalling. Nature. 2009;461(7264):614–20.

75. Park TS, Zimmerlin L, Evans-Moses R, Thomas J, Huo JS, Kanherkar R, et al. Vascular progenitors generated from tankyrase inhibitor-regulated Naïve diabetic human iPSC potentiate efficient revascularization of ischemic retina. Nat Commun. 2020;11(1):1195.

76. Drullinsky PR, Hurvitz SA. Mechanistic basis for PI3K inhibitor antitumor activity and adverse reactions in advanced breast cancer. Breast Cancer Res Treat. 2020;181(2):233–48.

77. Camps M, Rückle T, Ji H, Ardissone V, Rintelen F, Shaw J, et al. Blockade of PI3Kgamma suppresses joint inflammation and damage in mouse models of rheumatoid arthritis. Nat Med. 2005;11(9):936–43.

78. Jacot JL, Sherris D. Potential therapeutic roles for Inhibition of the PI3K/Akt/mTOR pathway in the pathophysiology of diabetic retinopathy. J Ophthalmol. 2011;2011:589813.

79. Takahashi S. Signaling effect, combinations, and clinical applications of triciribine. J Chemother. 2024:1–9.

80. Shan S, Liu F, Ford E, Caldwell RB, Narayanan SP, Somanath PR. Triciribine attenuates pathological neovascularization and vascular permeability in a mouse model of proliferative retinopathy. Biomed Pharmacother. 2023;162:114714.

81. Pearl NZ, Babin CP, Catalano NT, Blake JC, Ahmadzadeh S, Shekoohi S, et al. Narrative review of topiramate: clinical uses and Pharmacological cons iderations. Adv Ther. 2023;40(9):3626–38.

82. Yoneda S, Tanaka E, Goto W, Ota T, Hara H. Topiramate reduces excitotoxic and ischemic injury in the rat retina. Brain Res. 2003;967(1–2):257–66.

83. Campochiaro PA, Shah SM, Hafiz G, Heier JS, Lit ES, Zimmer-Galler I, et al. Topical mecamylamine for diabetic macular edema. Am J Ophthalmol. 2009;149(5):839–e851831.

84. El-Remessy AB, Rajesh M, Mukhopadhyay P, Horváth B, Patel V, Al-Gayyar MMH, et al. Cannabinoid 1 receptor activation contributes to vascular inflammation and cell death in a mouse model of diabetic retinopathy and a human retinal cell line. Diabetologia. 2011;54(6):1567–78.

85. Collier RJ, Patel Y, Martin EA, Dembinska O, Hellberg M, Krueger DS, et al. Agonists at the serotonin receptor (5-HT(1A)) protect the retina from severe photo-oxidative stress. Invest Ophthalmol Vis Sci. 2011;52(5):2118–26.

86. Kramerov AA, Saghizadeh M, Caballero S, Shaw LC, Li Calzi S, Bretner M, et al. Inhibition of protein kinase CK2 suppresses angiogenesis and hematopoietic stem cell recruitment to retinal neovascularization sites. Mol Cell Biochem. 2008;316(1–2):177–86.

87. Sparr HJ, Beaufort TM, Fuchs-Buder T. Newer neuromuscular blocking agents: how do they compare with established agents? Drugs. 2001;61(7):919–42.

88. Rüedi-Bettschen D, Spealman RD, Platt DM. Attenuation of cocaine-induced reinstatement of drug seeking in squirrel monkeys by direct and indirect activation of 5-HT2C receptors. Psychopharmacology (Berl). 2015;232(16):2959–68.

Publisher's note